Journal of Power Sources 226 (2013) 87–93

Contents lists available at SciVerse ScienceDirect

Journal of Power Sources

journal homepage: www.elsevier.com/locate/jpowsour

Characteristics of high-water-uptake activated carbon/Nafion hybrid membranes for proton exchange membrane fuel cells

Hung-Chung Chien [a], Li-Duan Tsai [a], Chien-Ming Lai [b], Jiunn-Nan Lin [b], Chao-Yuan Zhu [a,**], Feng-Chih Chang [a,c,*]

[a] Department of Applied Chemistry, National Chiao Tung University, Hsinchu 300, Taiwan
[b] Material and Chemical Research Laboratories, Industrial Technology Research Institute, Chutung, Hsinchu 310, Taiwan
[c] Department of Materials and Optoelectronic Science, National Sun Yat-Sen University, Kaohsiung, Taiwan

HIGHLIGHTS

- A cost-effective and high-throughput method for producing high-water-uptake membrane is developed.
- Activated carbon/Nafion hybrid membranes exhibit high-water-uptake and improved proton conductivity.
- The hybrid membrane displays a better performance to that of the commercial Nafion 211 when used in fuel cell measurements.
- The hybrid membranes reveal lower resistances during the operation of the PEMFC test.

ARTICLE INFO

Article history:
Received 8 October 2012
Accepted 9 October 2012
Available online 29 October 2012

Keywords:
Nafion
Activated carbon
Water uptake
Proton exchange membrane fuel cell

ABSTRACT

A cost-effective and high-throughput method for producing high-water-uptake membranes is developed by combining high-porosity and superior-surface-area activated carbon with Nafion. The resultant activated carbon/Nafion hybrid composite exhibits high water uptake and an improved proton conductivity, which can be exploited in a proton exchange membrane fuel cell (PEMFC). This hybrid membrane displays a superior performance to that of the commercial Nafion 211 when used in fuel-cell measurements. Electrochemical impedance spectroscopy (EIS) is used to simulate the changes in resistance during the operation of the fuel cells and conclusively explains the improved performance of the composite membranes.

1. Introduction

Fuel cells (FCs) are electrochemical devices that directly convert chemical energy into electrical energy. Among existing FC designs, the proton exchange membrane fuel cell (PEMFC) has generated immense interest because of its high power density, which is essential for widespread deployment in electric vehicles and residential power generation [1–3]. The proton exchange membrane (PEM) is critical to the performance of a PEMFC because it acts as a proton conductor and a fuel separator between the anode and cathode. Dupont's Nafion® is one of the most commonly used commercially available PEMs. However, dehydration at low relative humidity (RH) adversely affects the overall proton conductivity, thus compromising the overall fuel-cell efficiency [4–8]. In addition, the mechanical and dimensional stability of the polymer membranes at elevated temperatures are important, as they impose limitations on the operational environment of the PEMFC systems. To overcome these issues, many research groups have proposed the introduction of nano-fillers into the Nafion membrane to enhance their capability to maintain proper hydration. Nano-fillers such as ZrO_2, SiO_2, and TiO_2 particles have been incorporated into Nafion and have been shown to extend the working temperature range and mechanical properties of the membranes. In addition, morphological changes in the PEMFC upon addition of numerous nanofillers have been suggested to explain the improved performance at high temperature and low relative humidity [9–20]. However, poor dispersion, extensive swelling, and reduced proton conductivity are generally observed in the hybrid membranes, and this leads to deterioration of the performance and durability of the PEMFC [21,22].

* Corresponding author. Department of Materials and Optoelectronic Science, National Sun Yat-Sen University, Kaohsiung, Taiwan. Tel./fax: +886 3 5131512.
** Corresponding author. Tel.: +886 3 571-2121; fax: +886 3 5131512.
E-mail addresses: cyzhu@mail.nctu.edu.tw (C.-Y. Zhu), changfc@mail.nctu.edu.tw (F.-C. Chang).

0378-7753/$ – see front matter © 2012 Elsevier B.V. All rights reserved.
http://dx.doi.org/10.1016/j.jpowsour.2012.10.017

Carbon/Nafion composite membranes have been widely studied because of their interesting properties of mechanical reinforcement and outstanding water uptake. However, the limited loading percentage of conductive carbon restricts their application in fuel cells [23]. Commercial Nafion 117 infiltrated with carbon has been realized by in-situ hydrothermal carbonization, and the composite membranes exhibit extremely high conductivity and water uptake, but with an undesirable increase in thickness that reduces the performance of the fuel cell [24]. Aside from the infiltrated nanofiller/membrane, activated carbon (AC) has also been considered as a promising candidate for water storage because of its high porosity and superior surface area [25–28]. These excellent properties of mesoporous/microporous AC open up possible research avenues for its integration into fuel cells as the active component for efficient energy conversion. If these advantageous non-electrical conductive and porous properties of AC can be rationally integrated into PEMFC systems, hybrid films with uninterrupted carbon–carbon interfaces could be created. Using electrochemical impedance spectroscopy (EIS), we systematically compared PEMFCs employing AC/Nafion composite membranes and Nafion 211 membranes under different relative humidity test conditions.

2. Experimental

2.1. Material

AC with a surface area exceeding 1500 $m^2\ g^{-1}$ was purchased from Osaka Gas and was milled with fused Zirconia powder for 72 h before use. Nafion 211 membrane (25 μm) and 18% Nafion DE2020 dispersion were obtained from Ion power Inc., Delaware, United States. Platinum supported activated carbon (Pt/C) was purchased from Tanaka, Japan, without further purification. Concentrated nitric and sulfuric acid (HNO_3, Scharlau, 65%, pure; H_2SO_4, Scharlau, 95–98%) were used without further purification.

2.2. Preparation of proton exchange membrane

The AC was first oxidized by refluxing in a mixture of HNO_3/H_2SO_4 (1/5, v/v) at 80 °C for 24 h. Then the solution was diluted with deionized water (DI water) and the sediment was collected after centrifugation. The modified AC was iteratively washed with DI water until a pH value of 7 was reached. The product was dried in a vacuum oven at 50 °C. The surface functionalization was quantitatively characterized by XPS (X-ray photoelectron spectroscopy, Thermo VGESCAlab 250). To assemble the AC/Nafion hybrid membranes, 5 or 10 wt% of modified AC was added to the Nafion solution (DE2020) and ultrasonicated for an hour, followed by stirring for another 12 h to ensure uniformity. The resulting AC/Nafion ink was blade-coated onto glass substrates. The resulting film was dried at 50 °C for 24 h and post-cured at 140 °C for 2 h. After removing the solvent, the AC/Nafion composite membrane was soaked in 1 M $H_2SO_{4(aq)}$ at 80 °C for an hour to activate the proton substitution reaction. Finally, the activated membrane was immersed in a water bath preheated to 80 °C to fully remove the residual acid.

2.3. Membrane characterization

The membrane morphologies were characterized using SEM (JEOL JSM-6500F) and TEM (JEOL JEM-2100F). To stain the hydrophilic domains, the membrane was converted to its Pb^{2+} form by immersion in 1 N $Pb(AC)_{2(aq)}$ solution overnight and then rinsing with water. The membranes were dried under vacuum at 80 °C for 12 h and then sectioned into 50-nm slices using an ultramicrotome. The slices were picked up with 200-mesh copper grids for TEM observation.

The dimensional stability was measured with a TMA (Thermomechanical analyzer, Q400, TA Instruments, Delaware, United States) using a modification of previously described method [29]. In brief, the experiments were carried out with a temperature scan from 35 to 150 °C at a ramp rate of 10 °C min^{-1} under nitrogen.

The proton conductivity of the membranes was measured using electrochemical impedance spectroscopy (Solartron 1260 Impedance/Gain-Phase Analyzer, Solartron Analytical, United Kingdom) in a four-electrode configuration. The impedance was measured in the range 1 MHz to 0.1 Hz with a perturbation voltage amplitude 0.01 V. The membrane (1 cm in diameter) was sandwiched between two smooth stainless-steel disk electrodes in a cylindrical polytetrafluoroethylene (PTFE) holder. Further measurements under a combination of different humidity and temperature conditions were recorded in a Temperature & Humidity TEST Chamber (MHK, Terchy Environmental Technology Ltd., Taiwan), in which a 1-h equilibration period was allowed for before any measurements were performed. The resistance of the membranes was calculated from the intercept of the real axis in the intermediate frequency domain of the impedance spectrum. The proton conductivity was calculated according to the following equation.

$$\sigma = \frac{L}{AR}$$

where σ, L, A, and R refer to the ionic conductivity, sample thickness, cross-sectional area, and the resistance of the membranes, respectively [30].

To evaluate the water uptake (WU), the membranes were first immersed in DI water at room temperature for 24 h to ensure the membranes were fully saturated. Then, membranes were dried in a vacuum oven at 70 °C for 24 h and weighed. To calculate the WU, we use the following equation,

$$\mathrm{WU}\ (\%) = \frac{W_{\mathrm{wet}} - W_{\mathrm{dry}}}{W_{\mathrm{dry}}} \times 100$$

where WU (%), W_{wet}, and W_{dry} are the water uptake by weight percentage, the weight of the wet membrane, and the weight of the dry membrane, respectively [30].

2.4. Preparation of catalyst-coated membrane and single cell

An ultrasonic spray-coating system (Prism 300/400, Ultrasonic Systems Inc., Massachusetts, U.S.) was used to fabricate both the anodic and cathodic catalyst on pristine Nafion 211 and AC/Nafion composite membranes (i.e., catalyst-coated membrane, CCM). The inks for the anodic and cathodic catalyst layer were prepared by dispersing 46.1 wt% Pt/C and 20 wt% Nafion solution in a mixture of DI water and isopropyl alcohol (IPA) with a planetary mixer (Mazerustar KK-400W, KURABO Industries Ltd., Japan). The solid content of spraying catalyst ink was calculated to be around 5 wt%. The Pt loadings of the anode and cathode used in the spraying method were 0.4 and 0.5 mg cm^{-2}, respectively. The active area of the CCM was experimentally determined to be around 25 cm^2. Next, the CCM was sandwiched between two gas diffusion layers (GDLs) (Sigracet 10BC, SGL Technologies GmbH., Germany) to fabricate the membrane electrode assembly (MEA). The MEA was held and sealed tightly between two pieces of gasket by screwing them onto the graphite plates engraved with a double serpentine and counter flow channel. Subsequently, the whole unit was carefully sealed between the metal plates under uniform pressure.

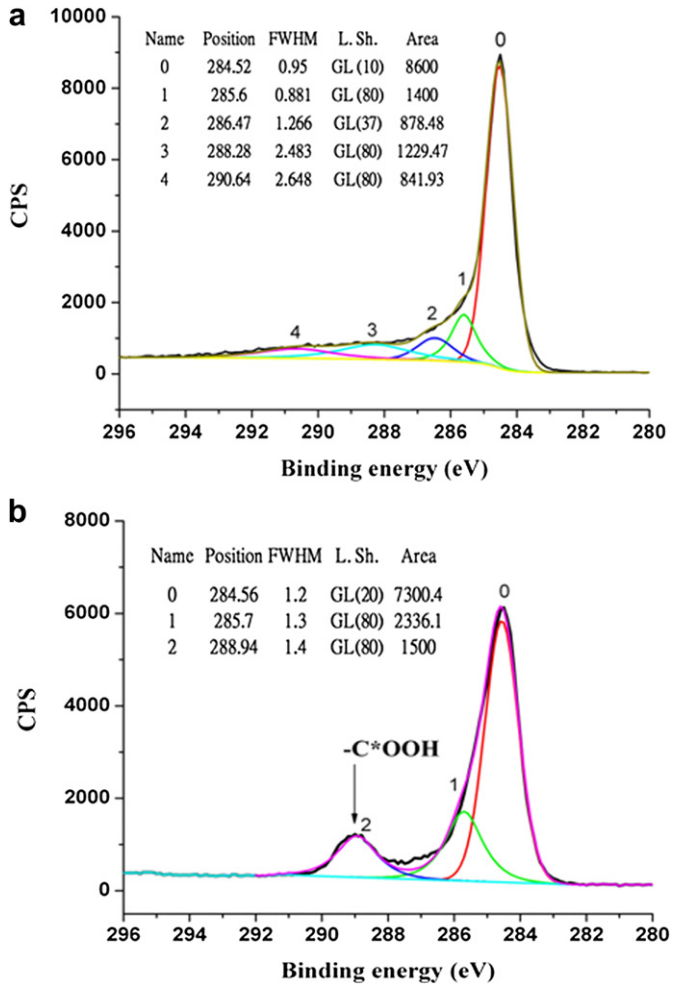

Fig. 1. XPS of the AC (a) before and (b) after extensive oxidization. A predominant peak at higher binding energy can be assigned to the carboxylic groups at the edges.

2.5. Characterization of I–V polarization and EIS

The current–voltage characteristics were measured using a multi-range fuel-cell test system (850e, Scribner Associates Inc. North Carolina, United States). I–V plots were obtained by potentiostatically decreasing the cell voltage stepwise at intervals of 0.025 V. The measurement of the I–V curve started from 0.85 V and each successive step was maintained for 60 s. The measurements were performed until the cell voltage reached 0.4 V.

EIS was performed at 800 mA cm^{-2} and was monitored using a multi-range fuel-cell test system equipped with a frequency response analyzer (FRA2 module). A two-electrode system was operated in the EIS by connecting a counter-electrode and the original anode (fed with hydrogen gas, hence referred to as a dynamic hydrogen electrode DHE) to the electrometer. The cathode (fed with air) was connected to the working electrode of the potentiostat. The impedance spectra were measured galvanostatically by inputting a sine wave with an amplitude of 10% of the DC current within a frequency range of 10 kHz–100 mHz. The analysis and curve fitting of the data were processed using the software Z-View.

While performing the I–V and EIS measurements, the PEMFC was operated at atmospheric pressure, with humid hydrogen being fed to the anode (stoichiometry: 1.5) at a humidification temperature of 45–70 °C, and humid air was fed to the cathode (stoichiometry: 2.0) at a humidification temperature of 45–70 °C. The operating temperature during the single-cell test was carefully maintained at 70 °C. The relative humidity of both sides of the single cell was carefully monitored throughout the measurement.

3. Results and discussion

3.1. Characterization of the composite membrane

XPS was used to analyze the chemical states of carbon in the modified AC. As shown in Fig. 1, a predominant C 1 s peak can be observed at 288.9 eV, which is characteristic of the carboxylic group. Additionally, the oxygen/carbon ratio substantially increases from the original 8.1/91.9 to 25.0/75.0, which is attributed to the extensive functionalization on the basal plane and at the edges that results in the AC being hydrophilic. The hydrophilicity of AC imparts solubility in common aqueous solvents. Moreover, the modified AC can be dispersed in Nafion without any observable precipitation after ultrasonication. The multiple hydrogen bonds between acidified carbon and sulfonic acid on Nafion keep the carbon well dispersed in the Nafion solution and also increase the viscosity.

The morphology of the prepared AC/Nafion composite membrane was further characterized using a combination of optical microscopy, scanning electronic microscopy (SEM), and transmission electron microscopy (TEM), as shown in Fig. 2. Fig. 2(a) shows an optical image of the freestanding 10% AC/Nafion membrane. Unlike transparent Nafion, the AC/Nafion hybrid membrane appears to be matted black and morphologically smooth in the macroscopic view. However, the SEM image, as shown in Fig. 2(b), provides a close-up view that reveals a rugged morphology with a large amount of sub-micron AC tethered to the

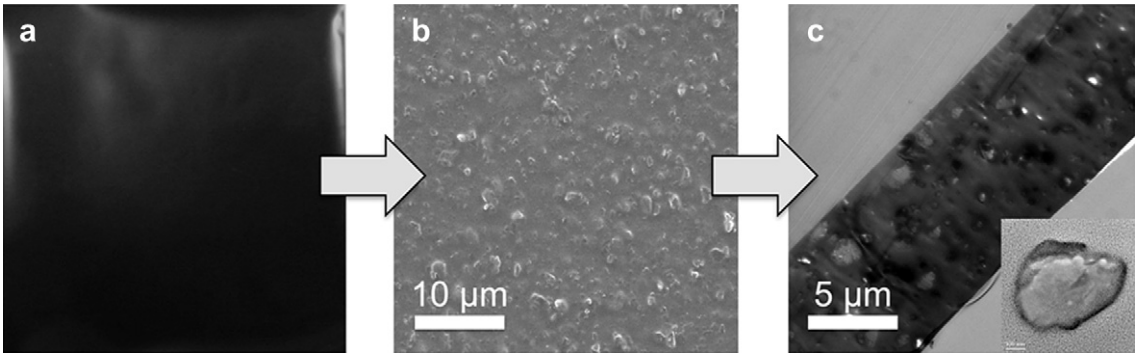

Fig. 2. (a) An optical image of a freestanding AC (10%)/Nafion film. (b) SEM and (c) TEM images provide close-up views of the microscopic morphology. Inset is the high-resolution TEM image of the distributed ionic domains.

Nafion framework. Fig. 2(c) shows a representative TEM image of the composite membrane along with an inset of a locally magnified dark region of hydrophilic ionic clusters stained with Pb^{2+} ions, while lighter patches represent hydrophobic moieties. It is these uniformly distributed micro-porous hydrophilic clusters that provide the improved capacity for the storage of water molecules, and thus ameliorate the dehydration problem under relatively low humidity conditions.

One of most important factors for the durability of the composite membrane is the dimensional stability of the membrane under elevated temperature. Fig. 3 shows the TMA plots of the percentage dimensional change versus temperature as a function of AC loading. From the curves, the dimensional change is greatly reduced as the carbon loading increases. The AC acts as filler with an extraordinarily high surface area that greatly enhances the strength of the composite membrane. The enhancement of the dimensional stability has been previously reported for various types of Nafion composite, including systems based on silica, clays, and graphite oxide [31,32]. In fuel-cell applications, a stiffer proton conductive material allows the use of thinner membranes with reduced internal resistance and without the risk of structural failure.

3.2. Percentage water uptake and proton conductivity of the membrane

The WU of the plain Nafion versus that of the activated carbon composite membranes is shown in Fig. 4. As the AC loading increases, the water uptake of the membrane is substantially enhanced. This can be explained by the formation of more hydrophilic channels and inherent micro/mesopores within the AC/Nafion hybrid membrane than within the pristine Nafion films. Structurally, Nafion has a backbone structure analogous to PTFE. However, unlike PTFE, Nafion is dressed with sulfonic acid ($SO_3^-H^+$) functional pendants, which provide charge sites for proton transport. In the AC/Nafion hybrid membrane, the abundant oxygen functional groups, which originated from extensive chemical modification, provide additional hydrophilic channels to facilitate ion transport in the presence of water. The WU of the pristine

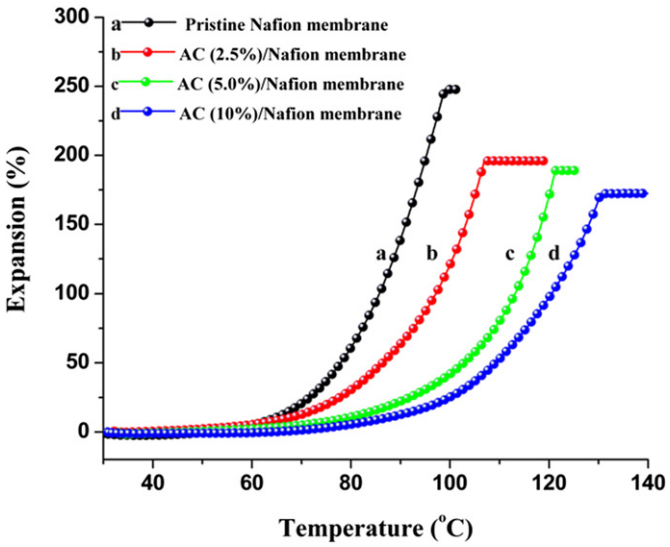

Fig. 3. Temperature dependence of the dimensional changes of the AC/Nafion hybrid composite with different chemically modified AC loads. The hybrid composite membrane loaded with 10% AC showed the smallest dimensional changes when tested at elevated temperatures.

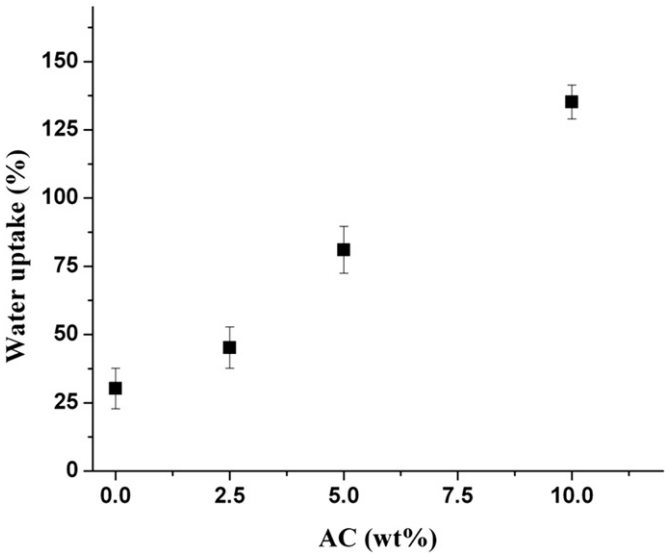

Fig. 4. The percentage water uptake as a function of different AC loadings of the AC/Nafion hybrid membrane. With increased loading of chemically modified AC, the hybrid membrane exhibited improved water uptake ability. (Water uptake experiments were conducted more than three times and error bars indicate deviations.)

Nafion recasted from DE2020 is measured to be around 30.3%, which is comparable to previously reported values [33]. However, the membrane embedded with 10% AC was found to exhibit a substantial increase in WU, as high as 135.2%, 4 times higher than that of the pure Nafion membrane. The composite membranes show reduced volume swelling ratios with high water uptake, which greatly enhances the stability of the composite membrane in different testing environments (see Supporting information Table S1).

The significantly improved WU in the hybrid membrane synergistically enhances charge transport, as sufficient hydronium ions can now propagate the aqueous phases. The conductivity of the Nafion and AC composite membranes is evaluated from

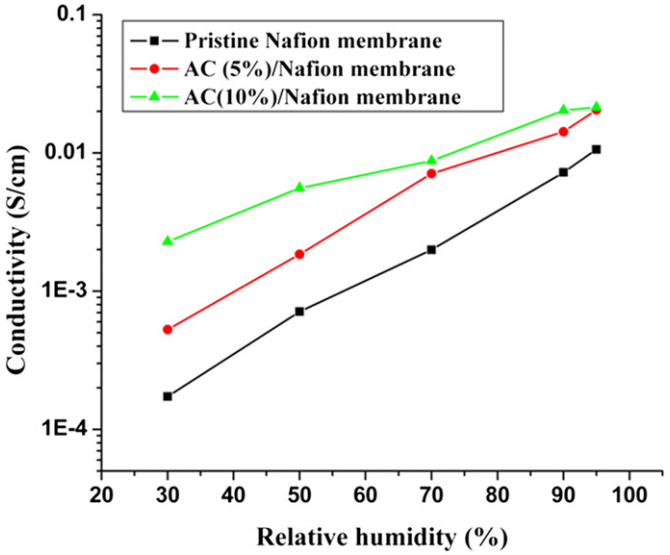

Fig. 5. Proton conductivity of the pristine Nafion 211 (black line), AC (5%)/Nafion (red line), and AC (10%)/Nafion (green line) hybrid membranes were recorded under different relative humidities. The hybrid membrane loaded with 10% chemically modified AC delivered superior conductivities at all relative humidities. (For interpretation of the references to colour in this figure legend, the reader is referred to the web version of this article.)

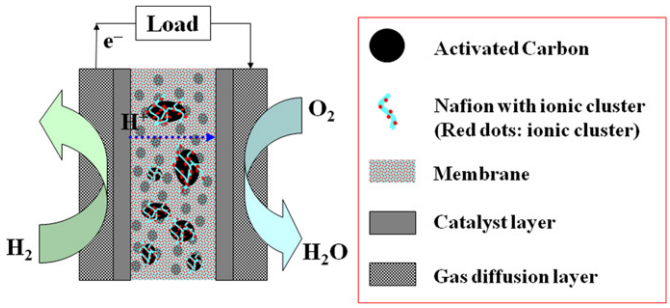

Fig. 6. Schematic illustration of the PEMFC setup used for fuel-cell measurements. The AC/Nafion hybrid membranes were used as a separator to disconnect the two catalyst layers.

impedance measurements. Fig. 5 conclusively shows the dependence of the conductivity on the varying relative humidity (RHs). The AC/Nafion composite membranes were found to possess superior conductivity to that of the Nafion membrane, especially at low RH. In the low RH range (30%), the pristine Nafion membrane gradually loses water content. As a result, the proton mobility drops significantly, leading to high resistance and low conductivity. However, the AC (10%)/Nafion composite membrane delivers higher conductivity owing to better water retention within in the largely porous and interconnected channels, preserving good quality interfaces that can propagate charge carriers.

3.3. Performance of the PEMFC under variable humidity conditions

Another important factor affecting the performance of fuel cells is the output characteristics under variable humidity conditions. A schematic illustration of the PEMFC with the AC composite membrane is shown in Fig. 6. Fig. 7 collectively shows the polarization curves at 70 °C for a PEMFC made of Nafion 211 and AC/Nafion composite membranes at different RHs. As illustrated in Fig. 7(a), the performance of the fuel cell made of Nafion 211 at low RH decreased drastically with decreasing RH. At a cell voltage of 0.65 V, fuel cells at different RHs exhibited current densities of 937.0 mA cm^{-2} (65% RH),

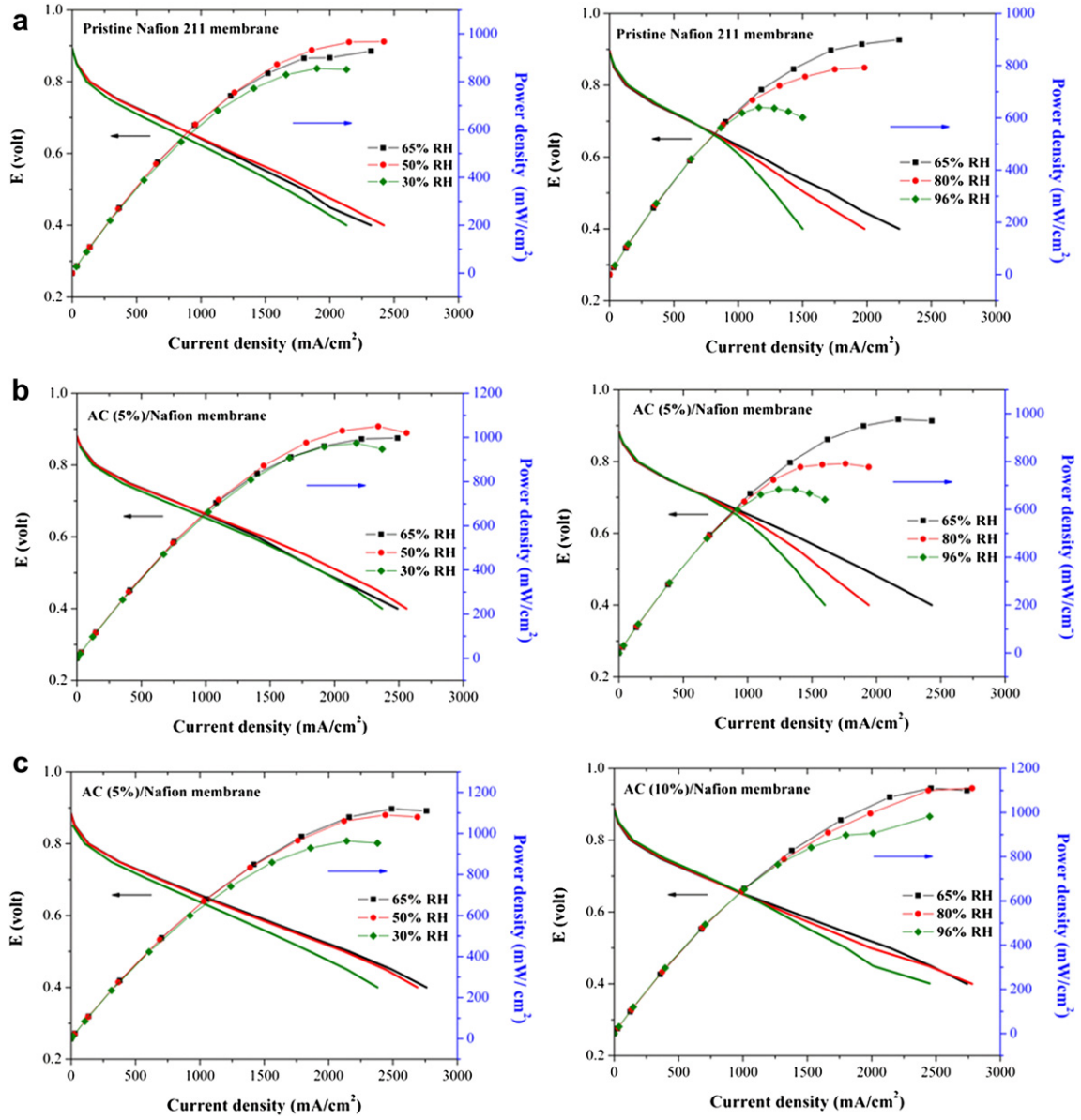

Fig. 7. Polarization curves of PEMFC with different AC loadings for (a) pristine Nafion 211, (b) AC (5%)/Nafion, and (c) AC (10%)/Nafion measured under relatively low (upper panel) and high humidity (lower panel). Different relative humidity test conditions were generated at 70 °C in the H_2/air system.

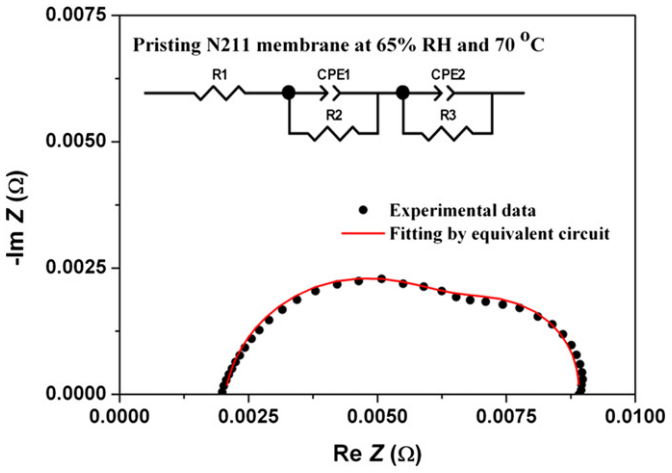

Fig. 8. Nyquist plot is plotted with the curve fitted based on the proposed equivalent circuit.

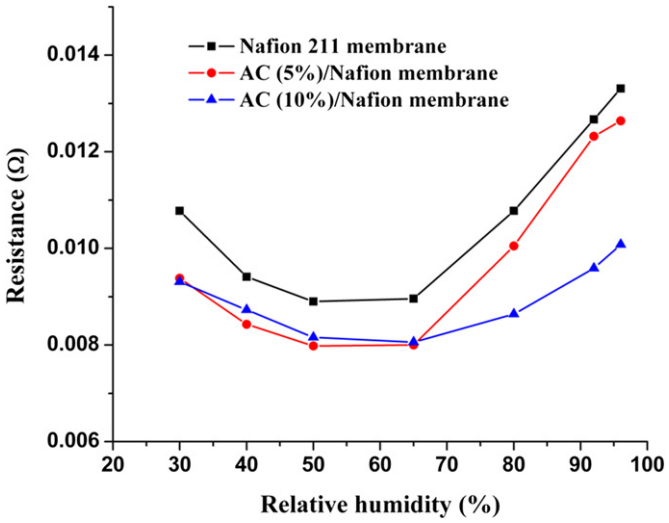

Fig. 10. Total resistance of the PEMFC measured under varying relative humidity.

950.7 mA cm^{-2} (50% RH), and 855.2 mA cm^{-2} (30% RH). The maximum power density of the fuel cell also decreased slightly from 924.0 to 860.4 mW cm^{-2} when the RH was reduced from 65% to 30%. Fig. 7(b) depicts the curves for a PEMFC with 5% AC measured at varying RH. At all RHs and at a cell voltage of 0.65 V, the current density remained in the range 1091.4 to 1013.5 mA cm^{-2} as the RH was decreased from 65% to 30%. The peak power density remained stable at around 1000 mW cm^{-2}. The performance of AC (10%)/Nafion was found to follow the same trend as the parent AC (5%)/Nafion and showed a stable current density and peak power density. The output characteristics of the AC composite membranes showed a higher and more stable current density and a higher peak power density than Nafion 211 at low RH, as a result of the high water uptake and better proton conductivity at low RH.

There are several factors that can account for the enhanced performance of the PEMFC at different RHs, including the ratio and the pressure of the air and H_2, the thermodynamics and kinetics of the catalyst, mass transfer, and membrane conductivity [34]. To better understand the role of the activated carbon in the membrane, fuel cells were also tested under conditions where the RH was increased from 65% to 95%. At relatively high RH, Nafion 211 delivered a stable current density at 0.65 V, discharging in the range of 886.6 to 860.9 mA cm^{-2} as the RH went from 65% to 95%. However, the power density decreased from 895.2 to 644.0 mW cm^{-2}. The dramatic reduction in power density is related to the flooding of the ionic channels in the catalyst layer under high RH conditions. In contrast, the AC (10%)/Nafion membrane displayed a stable performance in this series of experiments. The peak power density decreased from 1107.6 mW cm^{-2} at 65% RH to 983.2 mW cm^{-2} at 96% RH and the current density from 1001.7 to 986.1 mA cm^{-2}. The steady performance can be attributed to free water molecules absorbed by the AC, which keep the ionic channel at a moderate moisture level.

3.4. Electrochemical impedance spectroscopy of the PEMFC

In-situ EIS was employed to characterize the performance of the fuel cell by identifying the limiting factors arising from each constituent, including membrane resistance, reaction kinetics of the catalysts, and mass transfer under different test conditions. Fig. 8 shows a typical Nyquist plot of a PEMFC single cell under a discharging current density of 800 mA cm^{-2} at 65% RH and 70 °C. The plot depicts two distorted capacitive semicircles in the upper plane. The first capacitive loop in the higher frequency range is related to the electrochemical reaction and the second loop is closely related to the mass transfer reaction in the lower frequency range. The intersection point on the horizontal axis at higher frequency is usually attributable to the internal resistance of the cell. Often, a rough or porous surface can cause the capacitance to appear as a constant phase element (CPE), which is used in a model in place of a capacitor to compensate for the non-ideal conditions in the system [35]. Thus, a schematic model coupled with an equivalent circuit was proposed to describe the mechanism under investigation in this work, as shown in the inset of Fig. 8. R_1, R_2, and R_3 represent the internal resistance (R_s), the resistance of the electrochemical reaction (charge transfer) (R_{ct}), and the resistance

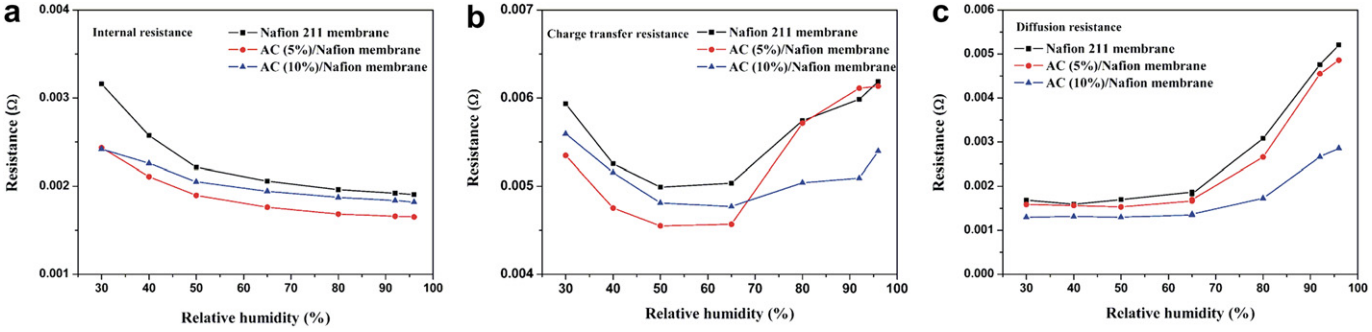

Fig. 9. (a) Internal resistance, (b) charge transfer resistance, and (c) diffusion resistance of the hybrid membranes with different loadings of AC measured at different relative humidity.

of the mass transfer reaction (diffusion) (R_{diff}), respectively, and CPE1 and CPE2 are constant phase elements of the charge transfer reaction (CPE_{ct}) and of the diffusion (CPE_{diff}), respectively [36]. The experimental EIS measurement is plotted with the theoretically predicted curve based on the proposed equivalent circuit shown in Fig. 8 and the fit is in good agreement.

The impedance of the simulated equivalent circuit at the discharge current density of 800 mA cm^{-2} was recorded and plotted as a function of the RH at 70 °C. Fig. 9(a) shows the internal resistance (R_s) for the PEMFC with the Nafion 211 and AC/Nafion hybrid membranes at different RHs. For the Nafion 211 and AC/Nafion hybrid membranes, R_s increased with decreasing RH. R_s refers to the internal resistance consisting of the PEM, contact loss, catalyst layers, and current collectors, which can be quantitatively characterized by EIS in the higher frequency range. Both 5% and 10% AC/Nafion composite membranes showed lower resistances than the pristine N211 membrane at the 30% RH, meaning that the AC/Nafion composite membranes can store water inside and thus maintain a high proton conductivity. The R_s results were found to be in agreement with the higher proton conductivity of the composite membranes at 30% RH shown in Fig. 4. However, the 10% composite membrane had a slightly higher resistance than that of the 5% composite membrane owing to higher surface roughness and higher ohmic contact resistance (see Supporting information Fig. S1).

Fig. 9(b) presents the charge transfer resistance as a function of RH. The charge transfer resistance (R_{ct}) can be understood by calculating the reactive area of the exposed Pt catalyst and the electrochemical reaction in the three-phase zones. The lowest resistance value was observed to be between 50 and 65% RH. Initially, the R_{ct} decreased as the RH decreased from 96% to 65% and below 65% RH, the resistance increased slightly. At low RH, the values of the R_{ct} are in the decreasing order: N211 > AC (10%)/Nafion > AC (5%)/Nafion. At high RH, the values of R_{ct} are in the decreasing order: N211 = AC (5%)/Nafion > AC (10%)/Nafion. The lowest R_{ct} and optimal operation condition for this PEMFC was at 65% RH at 70 °C, according to results of the simulation.

The diffusion resistance is related to the oxygen transport limitations in the GDL and the catalyst layer on the cathode side of the fuel cell. Fig. 9(c) shows the cathode diffusion resistance at the current density 800 mA cm^{-2} at 70 °C for various RHs. The resistance had a slight variation below 65% RH, which implies unhindered fuel penetration through the GDLs to the catalyst layer. However, as the RH increased above 65%, the resistance increased significantly owing to the excess water molecules adsorbed in the ionic channels, which could impede oxygen diffusion. The AC/Nafion composite membranes showed lower resistance than commercial Nafion 211, which indicates that the AC with high surface area and micro/mesoporous surface can reduce flooding, resulting in lower resistance.

Fig. 10 shows the total resistance of a fuel cell during operation, where the total resistance is the sum of R_s, R_{ct}, and R_{diff}. From these curves, the Nafion 211 membrane had the highest resistance during the FC test and the membrane containing 10% AC had the lowest resistance at various RHs. The results can be used to explain why the high-water-retention membranes (5% and 10% AC in the hybrid composites) showed higher and more stable current densities and higher peak power densities than Nafion 211.

4. Conclusions

A high-water-uptake AC/Nafion composite membrane was designed and operated under different test conditions, and electrochemical impedance spectroscopy was used to monitor changes in the resistance of the PEMFC. The 10% AC composite membrane showed superior current density and peak power density over the commercial Nafion 211 at various relative humidities. A simulation of the resistances during FC operation was used to explain the enhanced performance of the composite membranes. In addition, using activated carbon as the supporting framework was also found to improve the overall performance of the prepared fuel cells as a result of the intrinsically high surface area and porosity. With the wide variety of carbon-based nanomaterials, the strategy outlined here can be adapted for the production of highly efficient and robust composite thin films for efficient energy conversion.

Acknowledgment

The authors wish to acknowledge discussions with Dr. Vincent C. Tung, Assistant Professor, Department of Materials Science and Engineering, University of California, Merced.

Appendix A. Supplementary material

Supplementary material related to this article can be found at http://dx.doi.org/10.1016/j.jpowsour.2012.10.017.

References

[1] K.A. Mauritz, R.B. Moore, Chem. Rev. 104 (2004) 4535–4585.
[2] L. Carrette, K.A. Friedrich, U. Stimming, Fuel Cells 1 (2001) 5–39.
[3] S.K. Kamarudin, W.R.W. Daud, S.L. Ho, U.A. Hasran, J. Power Sources 163 (2007) 743–754.
[4] V. Baglio, A.S. Arico, A.D. Blasi, V. Antonucci, P.L. Antonucci, S. Licoccia, E. Traversa, F.S. Fiory, Electrochim. Acta 50 (2005) 1241–1246.
[5] S. Ren, G. Sun, C. Li, S. Song, Q. Xin, X. Yang, J. Power Sources 157 (2006) 724–726.
[6] R. Lanniello, V.M. Schmidt, U. Stimming, J. Stumper, A. Wallan, Electrochim. Acta 39 (1994) 1863–1869.
[7] A. Heinzel, V.M. Barragán, J. Power Sources 84 (1999) 70–74.
[8] Z.G. Shao, P. Joghee, I.M. Hsing, J. Membr. Sci. 229 (2004) 43–51.
[9] H. Tang, Z. Wan, M. Pan, S.P. Jiang, Electrochem. Commun. 9 (2007) 2003–2008.
[10] H. Nakajima, S. Nomura, T. Sugimoto, S. Nishikawa, I. Honma, J. Electrochem. Soc. 149 (2002) A953–A959.
[11] N.H. Jalani, K. Dunn, R. Datta, Electrochim. Acta 51 (2005) 553–560.
[12] F. Bauer, M. Willert-Porada, J. Power Sources 145 (2005) 101–107.
[13] O. Savadogo, J. Power Sources 127 (2004) 135–161.
[14] J.H. Tian, P.F. Gao, Z.Y. Zhang, W.H. Luo, Z.W. Shan, Int. J. Hydrogen Energy 33 (2008) 5686–5690.
[15] S.K. Young, W.L. Jarrent, K.A. Mauritz, Polymer 43 (2002) 2311–2320.
[16] M.V. Williams, H.R. Junz, J.M. Fenton, J. Power Sources 135 (2004) 122–134.
[17] M. Amirinejad, S. Rowshanzamir, M.H. Eikani, J. Power Sources 161 (2006) 872–875.
[18] H. Xu, Y. Song, H.R. Kunz, J.M. Fenton, J. Electrochem Soc. 152 (2005) A1828–A1836.
[19] K.C. Neyerlin, H.A. Gasteiger, C.K. Mittelsteadt, J. Jorne, W. Gu, J. Electrochem Soc. 152 (2005) A1073–A1080.
[20] W. Schmittinger, A. Vahidi, J. Power Sources 180 (2008) 1–14.
[21] S.M. Slade, J.R. Smith, S.A. Campbell, T.R. Ralph, C. Ponce de Leon, F.C. Walsh, Electrochim. Acta 55 (2010) 6818–6829.
[22] S.J. Peighambardoust, S. Rowshanzamir, M. Amjadi, Int. J. Hydrogen Energy 35 (2010) 9349–9384.
[23] Y.H. Liu, B. Yi, Z.G. Shao, D. Xing, H. Zhang, Electrochem. Solid-state Lett. 9 (2006) A356–A359.
[24] Z. Chai, C. Wang, H. Zhang, C.M. Doherty, B.P. Ladewig, A.J. Hill, H. Wang, Adv. Funct. Mater. 2 (2010) 4394–4399.
[25] Y.H. Li, C.W. Lee, B.K. Gullett, Carbon 40 (2002) 65–72.
[26] J. Gamby, P.L. Taberna, P. Simon, J.F. Fauvargue, M. Chesneau, J. Power Sources 101 (2001) 109–116.
[27] C.P. Huang, M.H. Wu, Water Res. 11 (1977) 673–679.
[28] Z. Jiang, Y. Liu, X. Sun, F. Tian, F. Sun, C. Liang, W. You, C. Han, C. Li, Langmuir 19 (2003) 731–736.
[29] Y. Iwai, T. Yamanishi, Polym. Degrad. Stab. 89 (2005) 43–49.
[30] Y.J. Huang, Y.S. Ye, Y.C. Yen, L.D. Tsai, B.J. Hwang, F.C. Chang, Int. J. Hydrogen Energy 36 (2011) 15333–15343.
[31] N. Cele, S. Ray, Macromol. Mater. Eng. 294 (2009) 719–738.
[32] S. Ansari, A. Kelarakis, L. Estevez, E.P. Giannelis, Small 6 (2010) 205–209.
[33] J.J. Yuan, H.T. Pu, Z.L. Yang, J. Polym. Sci. Part A: Polym. Chem. 47 (2009) 2647–2655.
[34] M.A. Hickner, H. Ghassemi, Y.S. Kim, B.R. Einsla, J.E. McGrath, Chem. Rev. 104 (2004) 4587–4612.
[35] N.Y. Hsu, S.C. Yen, K.T. Jeng, C.C. Chien, J. Power Sources 161 (2006) 232–239.
[36] G. Dotelli, L. Omati, P.G. Stampino, P. Grassini, D. Brivio, J. Power Sources 196 (2011) 8955–8966.